ORIGINAL

CrossMark

Designing an artificial neural network using radial basis function to model exergetic efficiency of nanofluids in mini double pipe heat exchanger

Nahid Ghasemi[1] · Reza Aghayari[2] · Heydar Maddah[2]

Abstract
The present study aims at predicting and optimizing exergetic efficiency of TiO_2-Al_2O_3/water nanofluid at different Reynolds numbers, volume fractions and twisted ratios using Artificial Neural Networks (ANN) and experimental data. Central Composite Design (CCD) and cascade Radial Basis Function (RBF) were used to display the significant levels of the analyzed factors on the exergetic efficiency. The size of TiO_2-Al_2O_3/water nanocomposite was 20–70 nm. The parameters of ANN model were adapted by a training algorithm of radial basis function (RBF) with a wide range of experimental data set. Total mean square error and correlation coefficient were used to evaluate the results which the best result was obtained from double layer perceptron neural network with 30 neurons in which total Mean Square Error(MSE) and correlation coefficient (R^2) were equal to 0.002 and 0.999, respectively. This indicated successful prediction of the network. Moreover, the proposed equation for predicting exergetic efficiency was extremely successful. According to the optimal curves, the optimum designing parameters of double pipe heat exchanger with inner twisted tape and nanofluid under the constrains of exergetic efficiency 0.937 are found to be Reynolds number 2500, twisted ratio 2.5 and volume fraction(v/v%) 0.05.

Keywords nanofluid · exergetic efficiency · radial basis function

1 Introduction

Energy saving is very important in the design, construction and operation of industrial heat exchangers. Exergy analysis is the relatively recent method to identify the location of maximum exergy destruction so that necessary action can be taken to increase the performance of the thermal system. Many researchers have attempted to increase the effective contact surface area with fluid to improve the heat transfer rate and to reduce the entropy generation. Therefore, energy saving is very important in the design, construction and operation of the heat exchangers [1, 2]. The second law of

thermodynamics targets energy balance. Exergy is the maximum useful work under the given environmental condition. It depends on the state of the system under consideration and state of environment. Inefficiencies in the process and place of inefficiencies can be very well identified using exergy analysis and thus, an exact place of improvement can be selected for overall improvement. Traditionally, thermodynamic analysis based on first law represents utilization of energy only. It does not provide any idea about losses and place of losses. Thus, application of exergy analysis has widely adopted in place of first law analysis. Based on the exergy analysis, various systems can be compared for thermodynamic inefficiencies. The performance of the system can be improved by identifying the area of maximum exergy destruction and modifying the design/ parameters to enhance the exergy efficiency [2]. Exergy analysis only suggests the area of maximum exergy destruction which can be modified. But along with exergy analysis, cost of modification and payback period is also essential. The overall cost of the system increases with increase in the exergetic efficiency. Thus, increase in the

✉ Nahid Ghasemi
    n-ghasemi@iau-arak.ac.ir; anahid3@gmail.com

1   Department of Chemistry, Arak Branch, Islamic Azad University, Arak, Iran

2   Department of Chemistry, Payame Noor University (PNU), P.O. Box 19395-3697, Tehran, Iran

economic cost of the system is followed by improvement in performance of the system. Thermo-economic analysis combines thermodynamic and economic analysis called exergy-economic analysis [2, 3].

Bhuvaet et al. [4] have tried to save energy by increasing the heat transfer coefficients in the cold and warm fluid sides in the heat exchangers. Twisted tapes are best passive techniques in literature. The effects of simple twisted tape and without twist insert on both working fluids flowing through the heat exchanger on exergy analysis parameter like effectiveness, entropy generation rate, entropy generation number and exergy loss are discussed and the effect of energy analysis parameter like overall heat transfer coefficient is also studied.

Maddah et al. [5] investigated heat transfer efficiency of water/iron oxide nanofluid in a double pipe heat exchanger equipped with a typical twisted tape experimentally. Experiments were conducted under the laminar and turbulent flow for Reynolds numbers in the range of 1000 to 6000 and the concentration of nanofluid was 0.01, 0.02 and 0.03 wt%. In order to model and predict the heat transfer efficiency, an artificial neural network was used. The temperature of the hot fluid (nanofluid), the temperature of the cold fluid (water), mass flow rate of hot fluid (nanofluid), mass flow rate of cold fluid (water), the concentration of nanofluid and twist ratio were input data in artificial neural network and heat transfer was output or target. Implementation of various structures of neural network with different number of neurons in the middle layer showed that 1–10-6 arrangement with the correlation coefficient 0.99181 and normal root mean square error 0.001621 is suggested as a desirable arrangement. In total, comparing the predicted results in this study with other studies and also the statistical measures shows the efficiency of artificial neural network.

Aghayari et al. [6] studied the effect of simultaneous use of nanofluids and perforated twisted tapes. In this work, the performance of water / iron oxide nanofluid in a double pipe heat exchanger with perforated twisted tapes is investigated under turbulent flow regime. The results showed that the addition of nanoparticles increases the heat transfer and the Nusselt number. Also, reducing the twist ratio (H/D = 2.5) of perforated twisted tape and using the nanofluid increase this value.

Maddah et al. [7] proposed new model to predict nanofluid thermal conductivity based on Artificial Neural Network. A two-layer perceptron feed forward neural network and back propagation Levenberg-Marquardt (BP-LM) training algorithm were used to predict the thermal conductivity of the nanofluid. The results show that ANN modeling is capable of predicting nanofluid thermal conductivity with good precision. The use of nanotechnology improves the heat transfer fluid and the cost is exorbitant.

Paisarn Naphon [8] has investigated experimentally and theoretically the entropy generation, exergy loss of a horizontal concentric micro-fin tube heat exchanger with a central finite difference method.

Yilmaz et al. [9] have studied double pipe heat exchanger based on second-law based analysis and evaluated the effect of entropy, exergy, entropy generation minimization and entropy generation number.

Ebrur and Bicer [10] have studied the effect of heat transfer rates, friction factor and exergy loss of various swirl generators having circular holes at different number and diameter on double pipe heat exchanger. The results show that heat transfer rates increase with decrease in diameter and with increase in number of holes on the swirl generators. Moreover, the dimensionless exergy loss and NTU increases with the increase in number of holes number and the decrease in diameter of hole.

Zhao et al. [11] introduced a novel viscosity prediction approach using artificial neural networks (ANN) as an alternative to the model-based viscosity prediction approach to estimate nanofluids viscosity. Radial basis function (RBF) neural networks was utilized to form viscosity prediction architectures. Alumina (Al_2O_3)-water nanofluids were used to test the effectiveness of the proposed method. The results showed that RBF neural network model had a reasonable agreement in predicting experimental data.

Li et al. [12] studied heat transfer enhancement and entropy generation of Al_2O_3-water nanofluids laminar convective flow in the micro-channels with flow control devices. The results revealed that the relative fanning frictional factor f/f_0 of the micro-channel with rectangle and protrusion devices are much larger and smaller than others, respectively. As the nanofluids concentration increases, f/f_0 increases accordingly. The micro-channels with cylinder and v-groove profiles have better heat transfer performance; especially at larger Re cases, while, the microchannel with the protrusion devices is better from an entropy generation minimization perspective. Furthermore, the variation of the relative entropy generation S_1/S_{10} are influenced by not only the change of Nu/Nu_0 and f/f_0, but also the physical parameters of working substances.

Ji et al. [13] investigated the entropy generation analysis of fully turbulent convective heat transfer to nanofluids in a circular tube numerically using the Reynolds Averaged Navier–Stokes (RANS) model. To confirm the validity of the numerical approach, the results have been compared with empirical correlations and analytical formula. According to the results, the intersection points of total entropy generation for water and four nanofluids are observed, when the entropy generation decreases before the intersection and increases after the intersection as the particle concentration increases.

In this work, Central Composite Design (CCD) and cascade Radial Basis Function (RBF) were used to estimate the exergetic efficiency of double pipe heat exchangers. The inputs include Reynolds number, volume fraction (ν/v) and twisted ratio(y/w). The exergetic efficiency of nanofluid is considered as output. Central Composite Design requires 20

experiments followed by ANOVA, F-test, and residue analysis to model the batch experimental system. In the present study, the experimental data are obtained by designing an ANN, which this is the novelty of this study.

2 Experimental

2.1 Experimental apparatus and method

The experimental investigation of heat transfer characteristic of nanofluid was carried out using the experimental apparatus as shown in Fig. 1. It mainly consists of a test section, receiving tanks in which working fluids are stored, heating and cooling system, flow meter, control and ball valve, pressure measurement system and data acquisition system. The working fluids were circulated through the loop by using variable speed pumps of suitable capacity. The test section is of 1200 mm length with counter flow path within horizontal double pipe heat exchanger in which hot nanofluid was applied inside the tube while cooling water was directed through the annulus. The inside pipe is made of a soft copper tube with the inner diameter of 6 mm, outer diameter of 8 mm and thickness of 1 mm while the outside pipe is of steel tube with the inner diameter of 14 mm,outer diameter of 16 mm m and

thickness of 1 mm. To measure the inlet and outlet temperature of the nanofluid and cold water at the inlet and outlet of the test section, 4 J-type thermocouples with precision 0.1 °C were used. This kind of thermocouple is used because of its high accuracy and resistance. All thermocouples were calibrated before fixing them. All four evaluated temperature probes were connected to the data logger sets. A 6 kW (kW) electronic heater and a thermostat installed on it were used to maintain the temperature of the nanofluid. During the test, the mass flow rate and the inlet and outlet temperatures of the nanofluid and cold water were measured. The temperature of inlet water was 20 ± 0.1 °C and the flow rate of the water was kept constant at 500 l/h.To measure the pressure drop across the test section, differential pressure transmitter was mounted at the pressure tab located at the inlet and outlet of the section. The nanofluid flow rate was measured by a magnetic flow meter which was placed at the entrance of the test section. For each test run, it was essential to record the data of the temperature, mass flow rates and pressure drop across the section at steady state conditions. Two storage tanks made of stainless steel with the capacity of 45 l were used to collect the fluids leaving the test section. Hot nanofluid was pumped from the fluid tank through the inner tube included twisted tapes at different Reynolds numbers of 1000 to 6000. To ensure the steady state condition for each run, the period of

Fig. 1 Experimental setup
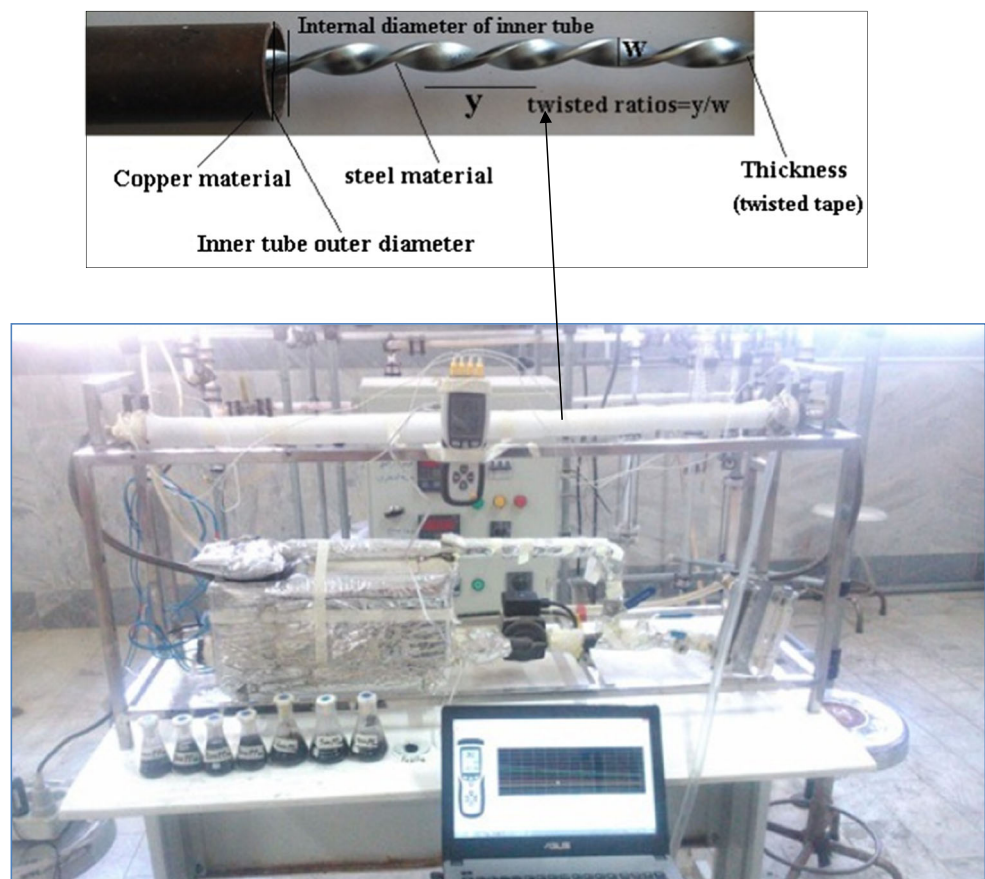
around 15–20 min, depending on Reynolds number and twisted tapes, was taken prior to the data record.

One type of twisted tape inserts made from stainless steel strips of thickness 12 mm were used.

2.2 Nanofluid preparation

The nanofluid was made by mixing in distilled water. TiO_2-Al_2O_3/water nanofluid with 0.01, 0.02, 0.03, 0.04 and 0.05% volume fraction were prepared as working fluids. Surfactant addition method was used for preparing nanofluid to this experimentation. Sodium Lauryl Sulphate (SLS) is used as surfactant. The method used for stabilizing the working fluid was magnetic stirring at 1500 rpm and ultra-sonication (20 KHz) for 1 h period to 1 l fluid. Figure 2 shows the scanning electron microscopy (SEM) micrograph of TiO_2-Al_2O_3/water nanocomposite. The average size of nanoparticles is estimated to be about 20–70 nm.

3 Data reduction

Heat transfer rate of the nanofluid was calculated from the difference between input and output temperatures of nanofluid as the following equation:

$$Q_{nf} = \dot{m}_{nf} Cp_{nf}(T_{out}-T_{in})_{nf} \tag{1}$$

where Q_{nf} is the heat transfer rate of the nanofluid and $\dot{m}_{nf}$ is the mass flow rate of the nanofluid. The heat transfer rate into the cooling water was calculated from the following equation:

$$Q_{bf} = \dot{m}_{bf} Cp_{bf}(T_{out}-T_{in})_{bf} \tag{2}$$

where Q_{bf} is the heat transfer rate of the base fluid and $\dot{m}_{bf}$ is the mass flow rate of the base fluid. T_{out} and T_{in} are respectively outlet and inlet temperature of base fluid.
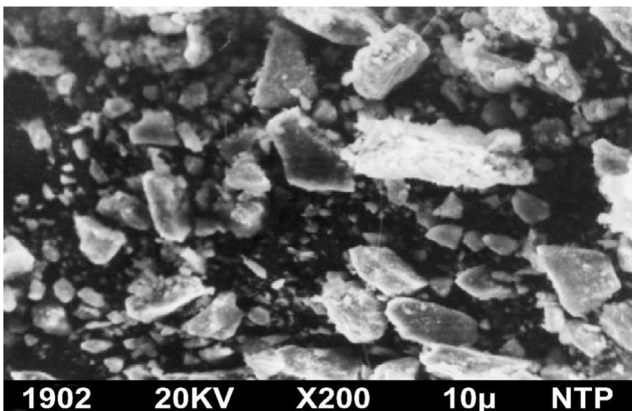

Fig. 2 SEM micrograph of the TiO_2-Al_2O_3/water nanocomposite

In this study, the supplied heat by the hot nanofluid was found to be 3% higher than the received heat. This deviation can be interpreted by convection and radiation heat loss along the test section. The average heat transfer rate Q_{ave}, is:

$$Q_{ave} = \frac{Q_{bf} + Q_{nf}}{2} \tag{3}$$

However, in this study, the exergy analysis does not include friction (or pressure drop) irreversibility and is based on only heat transfer irreversibility. The entropy generation rate can be written as follows [26]:

$$S_{generation} = \left(\dot{m}C_p\right)_{hot} \ln\frac{\left(T(hot)_{out}\right)}{\left(\left(T(hot)_{in}\right)\right)} \tag{4}$$
$$+ \left(\dot{m}C_p\right)_{cold} \ln\frac{\left(T(cold)_{out}\right)}{\left(\left(T(cold)_{in}\right)\right)}$$

Where $T(hot)_{out}$ is the outlet hot-side temperature, $T(hot)_{in}$ is the inlet hot-side temperature, $T(cold)_{out}$ is the outlet cold-side temperature, $T(cold)_{in}$ is the inlet cold-side temperature, in $\left(\dot{m}C_p\right)_{hot}$, $\dot{m}$ and C_p are respectively mass flow rate and specific heat at constant pressure of hot fluid and in $\left(\dot{m}C_p\right)_{cold}$, $\dot{m}$ and C_p are respectively mass flow rate and specific heat at constant pressure of cold fluid. The exergy efficiency or second law efficiency is as [26]:

$$E = 1 - \frac{C_{P,nf}(T_{out}-T_{in})-T_0 C_{P,nf}\ln\left(\frac{T_{out}}{T_{in}}\right)+\frac{\Delta P}{\rho_{nf}}}{C_{P,nf}(T_{in}-T_0)-T_0 C_{P,nf}\ln\left(\frac{T_{in}}{T_0}\right)+\frac{\Delta P}{\rho_{nf}}+C_{P,nf}(T_{out}-T_{in})\left(1-\frac{T_0}{T}\right)} \tag{5}$$

where ΔP is the measured pressure drop of the nanofluid, C_P is the specific heat, T_0 is the reference dead temperature and ρ_{nf} is the density of nanofluid.

4 Response surface methodology

In most RSM problems, the form of the relationship between the response and the independent variables is unknown. Thus, the first step in RSM is to find a suitable approximation for the true functional relationship between Y (response variable) and independent variables set. Usually, a low-order polynomial in some region of the independent variables is employed. If the response is well modeled by a linear function of the independent

variables, then the approximating function is the first-order model [27].

$$Y = \beta_0 + \sum_{i=1}^{k} \beta_i x_i + \varepsilon \qquad (6)$$

where Y is a response variable; k is the number of variables, β_0 is the constant term, β_i represents the coefficients of the linear parameters, x_i represents the variables, and ε is the residual associated to the experiments.

The next level of the polynomial model should contain additional terms, which describe the interaction between the different experimental variables. This way, a model for a second-order interaction presents the following terms [28]:

$$Y = \beta_0 + \sum_{i=1}^{k} \beta_i x_i + \sum_{i=1}^{k} \beta_{ii} x_i^2 + \varepsilon \qquad (7)$$

Where β_{ii} is a constant. In order to determine a critical point (maximum, minimum, or saddle), it is necessary for the polynomial function to contain quadratic terms according to the equation presented below [28]:

$$Y = \beta_0 + \sum_{i=1}^{k} \beta_i x_i + \sum_{i=1}^{k} \beta_{ii} x_i^2 + \sum_{1 \le i \le jk}^{k} \beta_{ij} x_i x_j + \varepsilon \qquad (8)$$

where β_{ij} is a constant, too. A second-order model can significantly improve the optimization process when a first order model suffers from lack of fit due to interaction between variables. For present study, factors and levels of process parameters are shown in Table 1.

The first requirement for RSM involves the design of experiments to achieve adequate and reliable measurement of the response of interest. To meet this requirement, an appropriate experimental design technique has to be employed. The experimental design techniques commonly used for process analysis and modeling are the full factorial, partial factorial and central composite designs. A full factorial design requires at least three levels per variable to estimate the coefficients of the quadratic terms in the response model. A partial factorial design requires fewer experiments than the full factorial design. However, the former is particularly useful if certain variables are already known to show no interaction. An effective alternative to factorial design is central composite design, requiring many fewer tests than the full factorial design and has been shown to be sufficient to describe the majority of steady-state process responses. Hence in this study, it was decided to use CCD to design the experiments. Hence, the total number of tests required for the three independent variables is $2^3 + 2 \times 3 + 6 = 20$ as shown in Table 2. [14]. All the experimental values are shown in Table 2.

5 Artificial neural networks

Due to their simplicity, flexibility, availability and large modeling capacity [15–17], the non-linear mathematical models of artificial neural network (ANN) get great attention. The processors are analogous to biological neurons in human brain. The feed forward neural network has been become the most popular in engineering applications [18, 19]. As shown in Fig. 4, this ANN configuration has one input layer, one hidden layer and one output layer. During the feed forward stage, a set of input parameter is supplied to the input nodes

Table 1 Experimental range and levels of independent variables

Coded factors	Parameters	Levels		
		-1	0	1
A	Reynolds number	2500	7250	12,000
B	Volume fraction (v/v %)	0.01	0.03	0.05
C	Twisted ratio(y/w)	2.5	3.85	5.2

Table 2 Experimental design in terms of coded factors and results of central composite design (CCD)

Std	Run	Factor 1 A:Reynolds number	Factor 2 B: volume fraction (v/v %)	Factor 3 C:twisted ratio(y/w)	Response 1 Exergetic efficiency
13	1	7250	0.03	2.5	0.53
5	2	2500	0.02	5.2	0.37
8	3	12,000	0.05	5.2	0.43
15	4	7250	0.03	3.85	0.61
1	5	2500	0.02	2.5	0.51
6	6	12,000	0.02	5.2	0.4
3	7	2500	0.05	2.5	0.92
7	8	2500	0.05	5.2	0.89
14	9	7250	0.03	5.2	0.55
17	10	7250	0.03	3.85	0.54
19	11	7250	0.03	3.85	0.55
16	12	7250	0.03	3.85	0.57
10	13	12,000	0.03	3.85	0.31
2	14	12,000	0.02	5.2	0.37
12	15	7250	0.05	3.85	0.43
20	16	7250	0.03	3.85	0.4
11	17	7250	0.02	3.85	0.33
9	18	2500	0.03	3.85	0.76
4	19	12,000	0.05	2.5	0.66
18	20	7250	0.03	3.85	0.54

Fig. 3 Architecture of the proposed ANN model for prediction
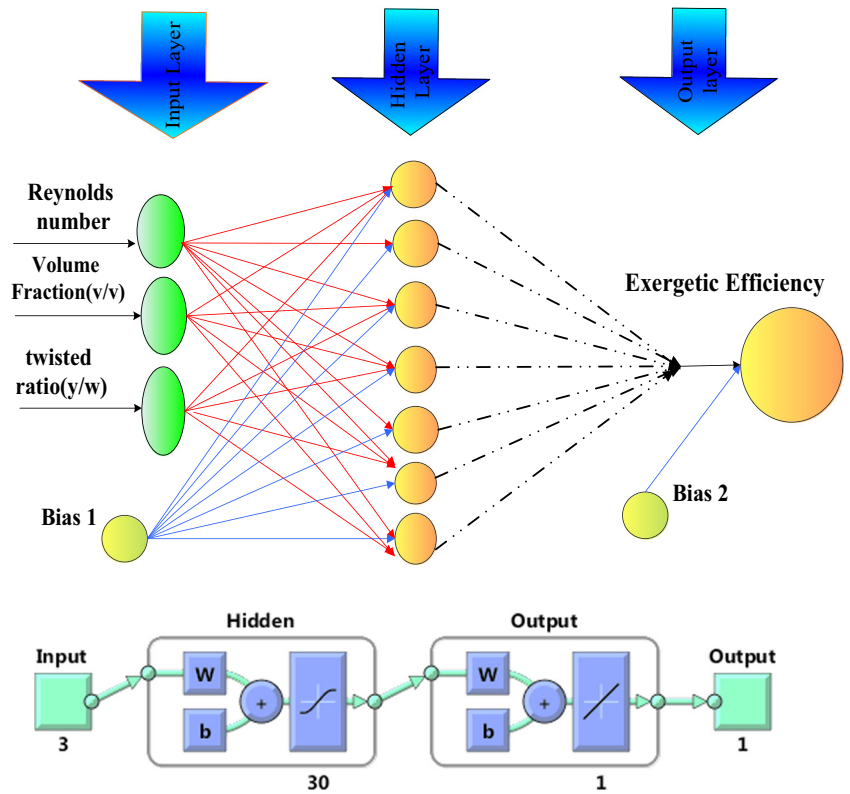

Fig. 4 Flow chart of RBF neural networks for exergetic efficiency prediction of nanofluids

and the information is transferred forward through the network to the nodes in the output layer. The nodes perform non-linear input–output transformations by means of sigmoid activation function. The mathematical background, the procedures for training and testing the optimize ANN model, and account of its history can be found in the text by Haykin [20]. In developing an ANN model, the available data set (70–80% of the data [21]) is divided into two dataset: the first dataset is used to train the ANN model, and then it is validated with another dataset. The training process of the ANN model can be done by comparing with the predicted results of the ANN model to the input data. The weights and biases are changed in order to minimize the error between the predicted output results and the input data. The scheme used in this study is the back propagation algorithm. The proposed ANN model configuration is set by selecting the number of hidden layer and the number of nodes in hidden layer. There are many training functions can be adopted in the training process, which the backward propagation algorithms are used in the present study. For all backward propagation algorithms, a three-layer ANN model with a tangent sigmoid transfer function (tansig) for hidden layer and a linear transfer function (purelin) for output layer are used. The Levenberg–Marquardt algorithm with a minimum MSE and R is used as the training function because of its higher stability and faster convergence rate. An artificial neuron is a basic processing element in modeling AANs and is characterized by weights (w), a bias (b), and a transfer/activation function (f). The weight values are set using a random number generator. The inputs to each neuron are multiplied by the weight values and the results are added with each other and with the
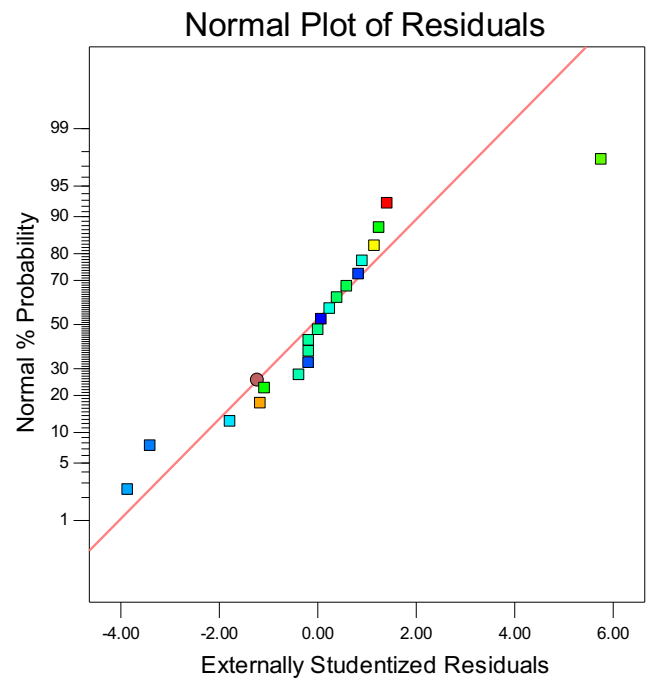

Fig. 5 Normal probability plots of residual for exergetic efficiency in mini double pipe heat exchangers

bias value. Then, the neuron output is extracted through a suitable transfer function according to Eq. (9).

$$Y_j = f\left(\sum_{i=1}^{n} w_{j,i} x_i + b_j\right) \qquad (9)$$

where x is the incoming signals, Y is the output and n is the number of neurons that connect to the jth neuron.

Table 3 Analysis of variance (ANOVA) for response surface quadratic model for exergetic efficiency

| Source	Sum of squares	df	Mean square	F -Value	p-value Prob > F	
Model	0.45	9	0.050	4.95	0.0099	Significant
A-Reynolds number	0.100	1	0.100	9.80	0.0107	Significant
B-volume fraction (v/v%)	0.11	1	0.11	11.01	0.0078	Significant
C-twisted ratio(y/w)	0.014	1	0.014	1.38	0.0469	Significant
AB	0.045	1	0.045	4.40	0.049	Significant
AC	1.414E-003	1	1.414E-003	0.14	0.0314	Significant
BC	1.682E-004	1	1.682E-004	0.017	0.0472	Significant
A^2	0.014	1	0.014	1.37	0.0212	Significant
B^2	0.019	1	0.019	1.83	0.0344	Significant
C^2	0.016	1	0.016	1.57	0.0293	Significant
Residual	0.10	10	0.010			
Lack of fit	0.076	4	0.019	4.40	0.0531	Not significant
Pure error	0.026	6	4.300E-003			
Cor total	0.55	19				
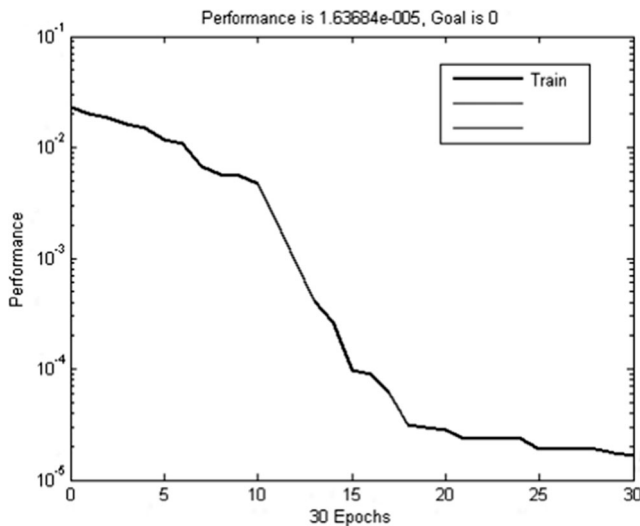
Fig. 6 Change of network performance with the number of iterations

5.1 Modeling method based on radial basis function (RBF) neural networks

The networks with radial circuit function are widely used to non-parametric estimation of a multi-dimension function via a limited set of training data. The radial neural networks due to their rapid and comprehensive learning are very helpful and particularly attractive [22]. It is worthy to note that these networks only by having one latent layer propose such properties. Often, these networks are compared with error post-propagation neural networks. The input layer is only an input layer and any processing doesn't occur there. The second layer or latent layer make a non-linear matching between input space and another space typically with a larger dimension and has an important role in converting the non-linear patterns to separable linear patterns. Finally, the third layer provides the weight sum along with a linear output. If it is used a RBF, this output will be useful but if necessary to classify the patterns, thus it can apply a rigid limiter or a sigmoid function on output neurons to produce the output values as 0 or 1. As it is clear from above explanations, the unique feature of this network is the processing that is done in latent layer. The function of latent layer can be expressed as follow:

$$F(x) = \sum_{j=1}^{p} w_j \varnothing \left(\| x - u_j \| \right) \qquad (10)$$

This relation shows that to estimating the f function from p function, a radius is used that has uj as centroid. The $\| x - u_j \|$ Symbol is a function of distance in space of R_n that typically is selected as Euclidian distance. Since that the curve of radial circuit functions has the radial symmetry, thus the neurons of latent layer is called as "radial function neurons". The famous function in radial networks is the Gussy or exponential function as follow:

$$\varnothing \left(\| x - u_j \| \right) = e^{\frac{\left(\| x - u_j \| \right)}{\sigma_j}} \qquad (11)$$

Where $\varnothing$ is the wide factor of j_{th} kernel, and u_j and σ_j are the center and width of the j_{th} RBF unit in the hidden layer, respectively. The Gauss exponential function selected as neurons response function in networks with radial circuit function because Girossi and Pougy in 1990 showed that the exponential function is belong to a group of functions that have best features for estimation. This ensures, there is a set of weights that estimates the relation between inputs and target vectors better than any other functions. This feature absent in sigmoid function that is used in designing the error post-propagation networks. An unsupervised learning stage is often used for adjusting the parameters of the hidden layer including RBF center c_i and width σ_i, and a supervised learning process is used to determine the connection weight ω_{ik} [23]. Up to now, a number of training algorithms have been proposed for training RBF networks, such as fixed randomly selected center, self-organized center selection and supervised selection of center [24]. As a self-organized method, orthogonal least square (OLS) approach has been employed for center selection [24, 25]. The OLS uses Gram–Schmidt algorithm for center selection and updating of RBF neural networks, and adaptive gradient descent procedure is used to adapt the weights [25]. The network parameters can be obtained by minimizing the following function:

$$minj = \sum_{k=1}^{q} |y_{nk} - y_{dk}|^2 \qquad (12)$$

where y_{nk} and y_{dk} are the network output and desire target output of the kth output layer node, respectively.

In the present study, data related to Reynolds number, volume fraction and twisted ratio were considered as input and exergetic efficiency was approved as target for the neural network (Fig. 3).

Table 4 Correlation coefficient (R) and MSE variation versus epochs for optimal ANN model in training, validation, test and all data with 30 neurons

Number of neuron	R^2				MSE			
	Test	Validation	Test	All	Training	Validation	Test	All
30	0.999	0.998	0.998	0.999	0.0001	0.0002	0.0003	0.0001

The progress trend is seen in Fig. 4. As seen, firstly the input and output data are given to network or selected. Then, the RBF neural network by its neurons initiates the test of trained network. Albeit, it should to say that in RBF neural networks, in addition to forming a network, the training process is occurs too. After training the network, based on specified maximum neurons and error rate that determined as default, if an acceptable answer obtained, it can say that training was success. Otherwise, by determine a different number of neurons and setting the default error rate differently, again the network training will perform to reach an acceptable answer. The RBF neural network model that adapted by Bromhear and Loo, needs to less training time and it can estimate the training vectors by zero error.

6 Uncertainty analysis

The uncertainties for different instruments and parameters used in experiment including thermocouple, flow meter, density, specific heat, Reynolds number and exergetic efficiency are estimated and their uncertainty persentages are ±0.15, ±0.19, ±0.13, ±0.16, ±0.23 and ±0.29, respectively.

7 Results and discussion

The calculated values of Exergetic Efficiency entered in the software design Expert 10. The response surface method is applied to develop the empirical relationship between experimental input variables and output responses such as Exergetic Efficiency. A regression analysis is done to develop the best fit model to the experimental data, which are used to generate response surface plots. Table 3 indicates the analysis of
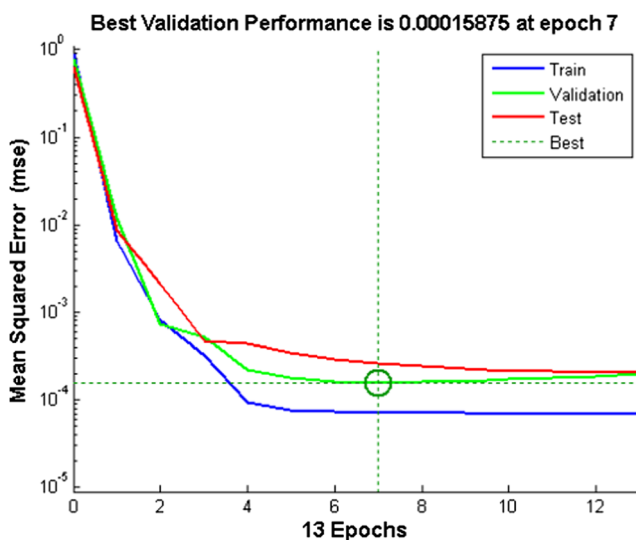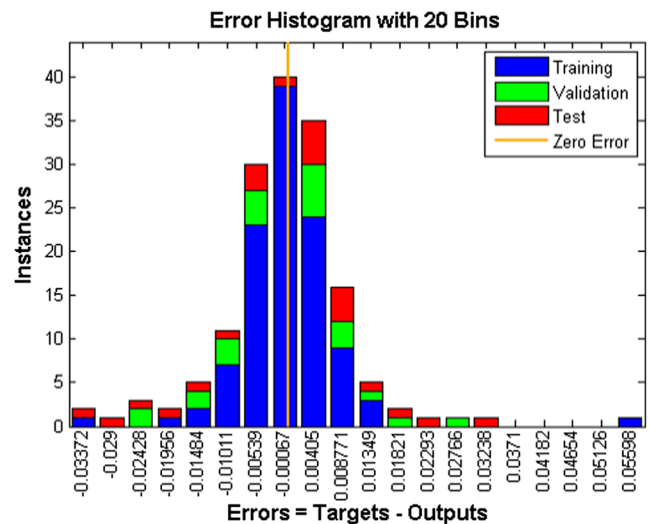

Fig. 8 Error histogram for training, validating and testing of the Simplified Model neural network for Exergetic Efficiency in mini double pipe heat exchangers

variance (ANOVA) for the output parameters of Exergetic Efficiency with double pipe heat exchanger. For the present study, Reynolds number (A) and twisted ratio (C) are generating significant effect than Volume fraction (B).The square valves of Reynolds number and twisted ratio have also major effect. The interaction effect between Reynolds number and Volume fraction of inclination (AB) has more impact on Exergetic Efficiency than Volume fraction and Twisted ratio (BC) and Reynolds number of inclination on the Twisted ratio (AC) on double pipe heat exchanger. For the double pipe heat exchanger, the predicted Model F–value of 4.04 suggests that the model is significant. There is only a 0.03% chance that a "Model F-Value" this large could occur due to noise. Values of "Prob > F" less than 0.05 reveal that model terms are significant. The "Pred R-Squared" of 0.9169 is not as close to the "Adj R-Squared" of 0.9365 as one might normally expect.
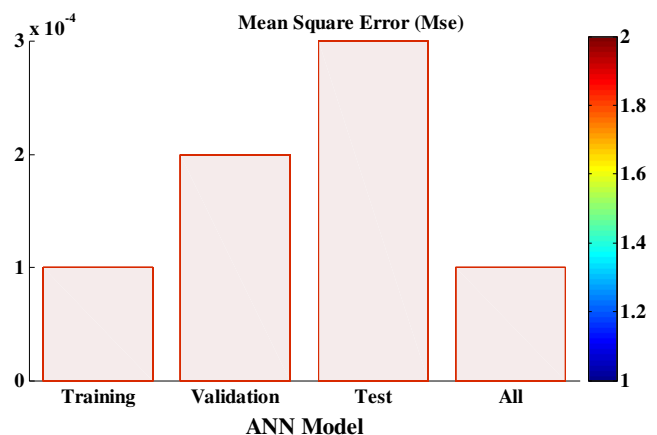

Fig. 7 The results of mean square error for exergetic efficiency data

Fig. 9 MSE variation versus epochs for optimal ANN model in training, validation, test and all data with 30 neurons
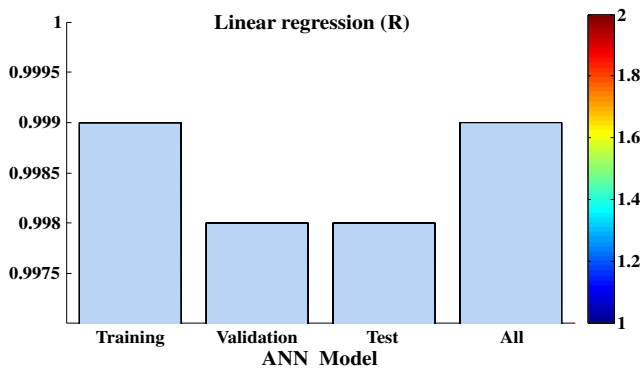
Fig. 10 R values of various ANN models for training, validation, test and all data with 30 neuron

This may indicate a large block effect or a possible problem with your model and/or data. The major parameters are model reduction, response transformation, outliers, etc. "Adeq Precision" measures the signal to noise ratio. Based on ANOVA and the following empirical relation is developed to predict the Exergetic Efficiency of double pipe heat exchanger. Regression equation in uncoded units is as following Equation:

$$
\begin{aligned}
Exergetic\ Efficiency = {} & 0.43331 - 1.63889E{-}005A + 44.37884B \\
& - 0.32980C - 1.26786E{-}003AB - 2.60882E \\
& - 006AC - 0.28499BC + 3.18848E{-}009A^2 \\
& - 369.15502B^2 + 0.042217C^2
\end{aligned}
$$

$$(13)$$

Other important information about fitting, reliability, adequacy and homogeneous and heterogeneous error variances of the models performance can be obtained in the diagnostic plots (Fig. 5). This Figure give show any deficiency of the models fitting to the experimental data. Figure 5 shows the normal probability of the residuals for responses, to confirm whether the standard deviations between the actual and the predicted response values follow a normal distribution. Points and points' clusters in Fig. 5 indicate that experimental values are distributed relatively near to the straight line and show desirable correlation between these values. Therefore, there are no serious violations in the hypothesis that errors are normally distributed and independent of each other, and also that the error variances are homogeneous and residuals are independent. The plots of residual against predicted responses. It can be observed that all points of experimental runs are randomly distributed and all values are within the range of −4 and 4. These results show that the models proposed by RSM are satisfactory and that the constant variance assumptions are confirmed.

Exergy efficiency was computed. Exergy efficiency in mini double pipe heat exchangers reduces with an increase in the Reynolds number. For optimum Reynolds number at 2500, at a particle volume fraction of 0.041%, TiO_2-Al_2O_3/water nanofluid exhibits the highest growth in as compared to water as base fluid. Exergetic Efficiency increases by increasing volume fraction of TiO_2-Al_2O_3/water and decreasing Reynolds number. When using nanofluids as agent fluid, it is known that, by adding different nanoparticles to the water, the Exergetic Efficiency increases. It can be said that the addition of nanoparticles in base fluids results into enhancement of the effective heat transfer surface area. Thermal conductivity increases because of the hydrodynamic effect of Brownian motion of nanoparticles, molecular level layering of the liquid at liquid particle interface, effect of nanoparticle clustering and the nature of the heat transport in nanoparticles [5]. With an increase in nanoparticles volume fraction, the viscosity of the nanofluids buildups and successively the fluid friction involvement in the Exergetic Efficiency rise. It is possible to observe that as Reynolds value increases, there is a reduction of Exergetic Efficiency, because there is a decrease in the difference between wall and bulk average temperatures, which causes a decrease in the Exergetic Efficiency [5]. Conversely, as Re increases, there is an increment of friction factor contribution on Exergetic Efficiency, due to the higher values of velocity gradient, causesing an increase in the wall shear stress [5]. Exergetic efficiency enhances between 18 and 56% using nanofluid and the loss decreased by 20–38%.Twisted tape inserts increases the heat transfer rate in the heat exchanger by increasing turbulence in the fluid flow. Turbulent flow or swirl flow increases the thermal contact by reducing boundary layer thickness. The turbulent flow ensures the better mixing of the fluid particles which increases heat transfer efficiency [5, 6].

Table 5 Range and responses for desirability

Name	Goal	Lower Limit	Upper Limit	Lower Weight	Upper Weight	Importance
A:Reynolds number	Minimize	2500	12,000	1	1	5
B:volume fraction(v/v%)	Maximize	0.02	0.05	1	1	5
C:twisted ratio(y/w)	Minimize	2.5	5.2	1	1	5
R:Exergetic Efficiency	Maximize	0.31	0.92	1	1	5

Table 6 Report of different desirabilities

Number	Reynolds number	Volume fraction (v/v%)	Twisted ratio (y/w)	Exergetic Efficiency	Desirability	
1	2500.000	0.050	2.500	0.937	1.000	Selected
2	2500.547	0.050	2.500	0.937	0.999	
3	2500.029	0.050	2.500	0.937	0.998	
4	2562.506	0.050	2.500	0.933	0.998	
5	2555.837	0.050	2.504	0.933	0.998	
6	2500.045	0.050	2.521	0.934	0.998	
7	2500.163	0.050	2.500	0.936	0.997	
8	2635.179	0.050	2.500	0.928	0.996	
9	2500.086	0.050	2.538	0.932	0.996	
10	2540.372	0.050	2.500	0.933	0.996	
11	2500.001	0.050	2.549	0.931	0.995	
12	2500.025	0.049	2.500	0.935	0.994	
13	2745.099	0.050	2.500	0.920	0.993	
14	2500.012	0.049	2.500	0.934	0.992	
15	2500.009	0.050	2.595	0.924	0.991	
16	2500.017	0.049	2.500	0.933	0.991	
17	2500.001	0.050	2.613	0.922	0.989	
18	2903.258	0.050	2.501	0.909	0.985	
19	2937.868	0.050	2.500	0.907	0.983	
20	2500.439	0.049	2.598	0.920	0.982	
21	2500.137	0.048	2.500	0.928	0.982	
22	2500.039	0.050	2.679	0.914	0.980	
23	2500.007	0.048	2.500	0.927	0.980	
24	3035.132	0.050	2.500	0.901	0.978	
25	2500.008	0.050	2.706	0.910	0.977	
26	2500.067	0.048	2.558	0.920	0.976	
27	2532.807	0.047	2.500	0.922	0.974	
28	2500.011	0.047	2.500	0.922	0.972	
29	2500.013	0.050	2.751	0.905	0.970	
30	3192.029	0.050	2.500	0.890	0.969	
31	2500.023	0.046	2.500	0.919	0.967	
32	3235.826	0.050	2.500	0.887	0.967	
33	2500.000	0.047	2.556	0.913	0.963	
34	3358.892	0.050	2.500	0.879	0.960	
35	3540.853	0.050	2.500	0.867	0.950	
36	2500.434	0.045	2.500	0.909	0.949	
37	2500.001	0.050	3.038	0.874	0.928	
38	2500.060	0.050	3.086	0.870	0.921	
39	2500.055	0.042	2.500	0.887	0.914	
40	2500.174	0.050	3.199	0.860	0.904	
41	2500.017	0.044	2.755	0.869	0.901	
42	2500.010	0.050	3.594	0.835	0.846	
43	2500.014	0.050	3.655	0.832	0.837	
44	2500.001	0.035	2.500	0.797	0.792	
45	2500.008	0.036	2.797	0.782	0.781	
46	2500.001	0.042	3.770	0.779	0.739	

As seen in Fig. 6, the change in network efficiency has been shown against repeat rate in network. Firstly, network assumes the default error rate as zero (goal = 0). However, it can change this value arbitrary so that it can consider a rate of error and when network reached to it, it will stop. By increase the repeat rate, the error rate will reduce. In Fig. 6, the repeat rate is 30 and the network performance for this rate reached to 1.63684e-005 that is an indication of successful prediction.

Table 4 shows the correlation coefficient (R) and MSE variation versus epochs for optimal ANN model in training, validation, test and all data with 30 neurons. In the science of statistics, dispersion is typically shown by correlation coefficient. If correlation coefficient is close to one, then this indicates that the predicted values for the model and what measured in the laboratory are the same. One of the problems occurs for neural networks with low number of data in training is "overfitting" phenomenon in which the model cannot be generalized. Evaluation of error for testing and accuracy data is one of the ways to recognize the overfitting [5]. Proximity of the correlation coefficient for this type of data reveals that overfitting did not take place. According to Table 4, the correlation coefficient for the data equals to 0.999, indicating that this phenomenon did not happen in our model.

Figure 7 is the performance plots of the mean square error value versus the number of epochs that is iteration numbers. Mean square error decreases with increasing iteration numbers and converges to a steady state value based on the Levenberg–Marquardt algorithm characteristic as the best training performance is achieved at 7 epochs [5].

Furthermore, the errors between output and target data, for training, validation and test data for Exergetic Efficiency in mini double pipe heat exchangers is represented in Fig. 8. As seen in the histograms, shape of the neural networks' errors is bell curve. For the Simplified Model, 86% of the training errors are focused between −0.01956 and 0.01349 and 73% of the validation errors are focused between −0.02428 and 0.01821 and 62% of the test errors are concentrated between −0.03372 and 0.03238. Although the maximum absolute error between the output and target is 0.05598, it's happening is clearly insignificant compared to data bank used as shown by Fig. 8. These comparative results show that optimal ANN architecture is 3–30-1. It is obvious that the percentage difference (%) between experimental and ANN results during training is in the range of (−0.058) to (+0.038).

Figures 9 and 10 represent the variation of mean square error (MSE) and correlation coefficient (R) of the optimized ANN model with number of 1 hidden layer with 30 neurons for testing and overall (training +testing) and validation dataset for Exergetic Efficiency in mini double pipe heat exchangers. It can be said that the MSE and R values tend to decrease and to increase with increase in the neurons hidden layer. With 1 hidden layer and 30 neurons, the MSE has it
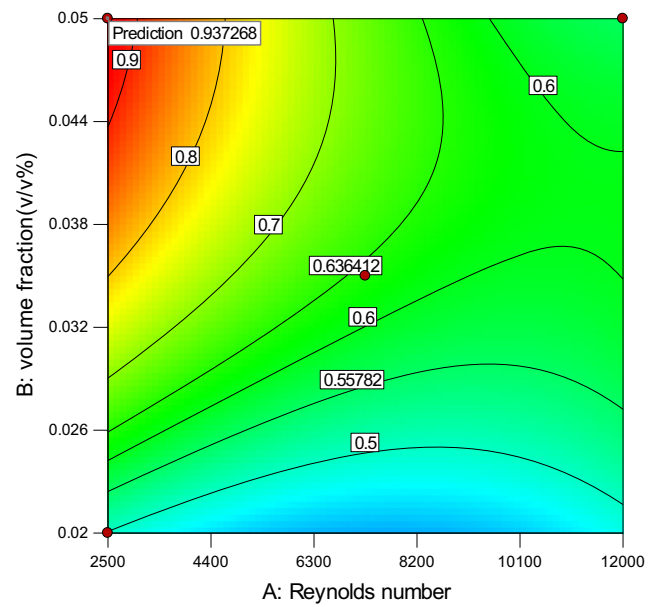

Fig. 11 Optimum graphs for exergetic efficiency

minimum value as well as maximum R. When the number of neurons is more than 30, the MSE and R increase and decrease, respectively [5]. Therefore, the neural network containing 1 hidden layer with 30 neurons is selected as the best case. Obviously, the best result is obtained by 30 neurons with 1 hidden layer. If the mean square error is smaller, the prediction will be successful [5].

The purpose of optimization is to find a right set of conditions that will meet the goals. Table 5 represents the ranges and responses for desirability. Here, Reynolds number and twisted ratio(y/w) is minimized and volume fraction (v/v%) is maximized. Exergetic Efficiency should be maximum for
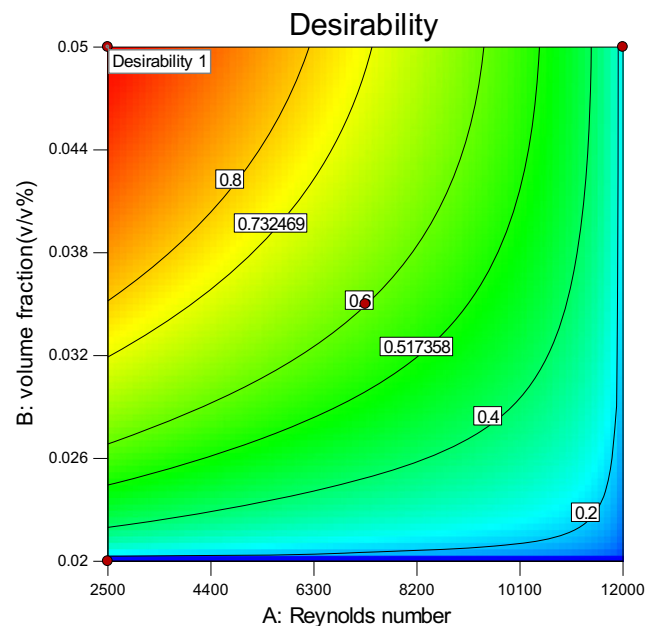

Fig. 12 Desirability graphs for exergetic efficiency

increased heat transfer rate. The appropriate set of conditions having highest desirability value is elected as optimum value. The highest desirability value in Table 6 and Figs. 11 and 12 is 1. Therefore, this set of conditions has been established as the optimum value.

8 Conclusion

The present study has been done on TiO_2-Al_2O_3/water nanocomposite. The main concern of experiment was to evaluate the nanoparticles volume fraction, Reynolds number and twisted ratio effect on the Exergetic Efficiency with inserting twisted tape. Central Composite Design (CCD) and cascade Radial Basis Function (RBF) were used to display the significant levels of the analyzed factors on the Exergetic Efficiency. Reynolds number, volume fraction and twisted ratio were considered as input and Exergetic Efficiency was approved as target for the neural network. Total mean square error and correlation coefficient were used to evaluate the results which the best result was obtained from double layer Perceptron Neural Network with 30 neurons in which total mean square error and correlation coefficient were equal to 0.002 and 0.999 respectively. Exergetic efficiency improved by 18% to 56% using nanofluid and the loss decreased by 20–38%. The optimum designing parameters of double pipe heat exchanger with inner twisted tape and nanfluid under the constrains of Exergetic Efficiency 0.937 are found to be Reynolds number 2500, twisted ratio(y/w) 2.5 and volume fraction (v/v%) 0.05.

References

1. Singh PK, Anoop KB, Sundararajan T, Das S (2010) Entropy generation due to flow and heat transfer in nanofluids. Int J Heat Mass Transf 53:4757–4767
2. Karami M, Shirani E, Avara A (2012) Analysis of entropy generation, pumping power, and tube wall temperature in aqueous suspensions of alumina particles. Heat Transfer Res 43(4):327–342
3. Oztop FH, Abu-Nada E (2008) Numerical study of natural convection in partially heated rectangular enclosures filled with nanofluids. Int J Heat Fluid 29:1326–1336
4. Bhuva BV, Soni S (2015) Experimental investigation of Exergy & energy analysis of double pipe heat exchanger using twisted tape. Int J Sci Res Dev| 3(4):2321–0613
5. Maddah H, Ghasemi N (2017) Experimental evaluation of heat transfer efficiency of nanofluid in a double pipe heat exchanger and prediction of experimental results using artificial neural networks. Heat Mass Transf:1–14. https://doi.org/10.1007/s00231-017-2068-6
6. Aghayari R, Maddah H, Baghbani Arani B, Mohammadiun H, Nikpanje H (2015) An experimental investigation of heat transfer of Fe_2O_3/water nanofluid in a double pipe heat exchanger. Int J Nano Dimensions 6(5):517–524
7. Hosseinian Naeini A, Baghbani Arani J, Narooei A, Aghayari R, Maddah H (2016) Nanofluid thermal conductivity prediction model based on artificial neural network. Trans Phenom Nano Micro Scales 4(2):41–46
8. Naphon P (2011) Study on the Exergy loss of the horizontal concentric micro-fin tube heat exchangers. Int Commun Heat Mass Transfer 38:229–235
9. Yilmaz M, Sara ON, Karsli S (2001) Performance evaluation criteria for heat exchangers based on second law analysis. Exergy Int J 1(4):278–294
10. Naphon P (2006) Second law analysis of the heat transfer of the horizontal concentric tube heat exchanger. Int Commun Heat Mass Transfer 1029–1041
11. Ningbo Z, Li S, Zhitao W, Yunpeng C (2014) Prediction of viscosity of nanofluids using artificial neural networks. Heat Transfer and Thermal Engineering. https://doi.org/10.1115/IMECE2014-40354
12. Li P, Xie Y, Zhang D, Xie G (2016) Heat transfer enhancement and entropy generation of nanofluids laminar convection in microchannels with flow control devices. Entropy 18(134):1–15
13. Yu J, Zhang H-C, Xie Y, Shi L (2017) Entropy generation analysis and performance evaluation of turbulent forced convective heat transfer to nanofluids. Entropy 19(108):1–18
14. Myers R (1976) Response Surface Methodology. Edwards Brothers, Ann Arbor, MI
15. Haykin S (1999) Neural networks: a comprehensive foundation, 2nd edn. Prentice Hall PTR, Upper Saddle River
16. Xu P, Xu S, Yin H (2007) Application of delf-organization competitive neural network in fault diagnosis of suck rod pumping system. J Pet Sci Eng 58:43
17. Vaferi B, Rahnam Y, Darvishi P, Toorani AR, Lashkarbolook M (2013) Phase equilibrium estimation of binary systems containing ethanol using optimal feed forward neural network. J Supercrit Fluids 84:80
18. Sreekanth S, Ramasamy HS, Sablani SS, Prasher SO (1999) A neural network approach for evaluation of surface heat transfer coefficient. J Food Process Preserv 23:329–348
19. Parcheco VA, Sen M, Yang KT, Meclain RL (2001) Neural network analysis of fin-tube refrigerating heat exchanger with limited experimental data. Int J Heat Mass Transf 44(4):763–770
20. Haykin S (1994) Neural networks, a comprehensive foundation, 1st edn. Prentice Hall PTR, Upper Saddle River
21. Aydinalp M, Ugursal VI, Fung AS (2001) Predicting residential appliance, lighting, and space cooling energy consumption using neural networks. Proceeding of ITEC2001, International Thermal Energy Congress Cesme Turkey 417
22. Hartman E, Keeler JD, Kowalski JM (1990) Layered neural networks with Gaussian hidden units as universal approximations. Neural Comput 2(2):210–215
23. Montazer GA, Khoshniat H, Fathi V (2013) Improvement of RBF neural networks using Fuzzy-OSD algorithm in an online radar pulse classification system. Appl Soft Comput 13(9):3831–3838
24. Iliyas SA, Elshafei M, Habib MA, Adeniran AA (2013) RBF neural network inferential sensor for process emission monitoring. Control Eng Pract 21(7):962–970
25. Chen S, Cowan CFN, Grant PM (1991) Orthogonal least squares learning algorithm for radial basis function networks. IEEE Trans Neural Netw 2(2):302–309
26. Mmohammadiun M, Dashtestani F, Alizadeh M (2016) Exergy prediction model of a double pipe heat exchanger using metal oxide nanofluids and twisted tape based on the artificial neural network approach and experimental results. J Heat Transf 138:1–10
27. Box GEP, Draper NR (1975) Robust Designs. Biometrika 62:347–352
28. Hunter WG, Hunter JS (1978) Statistics for experimenters: an introduction to design, data analysis, and model building. Wiley, New York, NY